

NAVAL POSTGRADUATE SCHOOL

Monterey, California



THESIS

**FUTURE SATELLITE TECHNOLOGY
THE ROLE OF NANOELECTRONICS**

by

John S. Rice

September 1998

Thesis Advisor:
Co-Advisor:

James H. Luscombe
Robert L. Armstead

19981110145

Approved for public release; distribution is unlimited.

REPORT DOCUMENTATION PAGE

Form Approved OMB No. 0704-0188

Public reporting burden for this collection of information is estimated to average 1 hour per response, including the time for reviewing instruction, searching existing data sources, gathering and maintaining the data needed, and completing and reviewing the collection of information. Send comments regarding this burden estimate or any other aspect of this collection of information, including suggestions for reducing this burden, to Washington Headquarters Services, Directorate for Information Operations and Reports, 1215 Jefferson Davis Highway, Suite 1204, Arlington, VA 22202-4302, and to the Office of Management and Budget, Paperwork Reduction Project (0704-0188) Washington DC 20503.

1. AGENCY USE ONLY (<i>Leave blank</i>)	2. REPORT DATE	3. REPORT TYPE AND DATES COVERED			
	September, 1998	Master's Thesis			

NSN 7540-01-280-5500

Standard Form 298 (Rev. 2-89)
Prescribed by ANSI Std. Z39-18 298-102

Approved for public release; distribution is unlimited.

**FUTURE SATELLITE TECHNOLOGY
THE ROLE OF NANOELECTRONICS**

John S. Rice
Lieutenant, United States Navy
B.S., United States Naval Academy, 1992

Submitted in partial fulfillment
of the requirements for the degree of

MASTER OF SCIENCE IN APPLIED PHYSICS

from the

NAVAL POSTGRADUATE SCHOOL

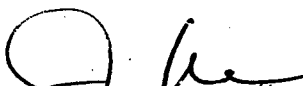
September 1998

Author:



John S. Rice

Approved by:


James Luscombe, Thesis Advisor

Robert Armstead, Co-Advisor



William B. Maier II, Chairman

Department of Physics

ABSTRACT

Tiny earth-orbiting spacecraft known as nanosatellites are now possible due to breakthroughs in microelectromechanics that permit engineers to build extremely small yet fully functional devices. With today's satellite launch costs averaging around \$20,000 per pound lifted into space, nanosatellites could revolutionize the future of space access by significantly reducing the size, mass, power requirements, complexity and ultimately the costs of space systems. The small satellite concept fosters a faster evolution in space science and introduces and tests state-of-the-art space technology. Of the technologies required to design a miniaturized and yet autonomous vehicle, nanoelectronics is at the forefront.

The field of nanoelectronics is primarily concerned with integrated circuit (IC) technology for scale sizes well below 100 nanometers. It is in this realm that the quantum mechanical nature of the electron becomes of paramount importance. With the tools of quantum physics, reduction in the size of individual transistors has yielded the quantum dot, a three-dimensional structure for confinement of a single electron. The theoretical study in this thesis will show that the width in p-n junctions is generally underestimated for curved interfaces by textbook formulas. This result is significant for semi-cylindrical quantum dots which are the logical result of continued down scaling in semiconductor devices.

TABLE OF CONTENTS

I.	INTRODUCTION.....	1
II.	NANOSATELLITE APPLICATIONS.....	3
	A. WHAT IS A NANOSATELLITE ?.....	3
	B. ADVANTAGES OF NANOSATELLITES.....	4
	1. Cost.....	4
	2. Redundancy.....	5
	3. Utility.....	6
III.	NANOTECHNOLOGY IN SMALL SATELLITES.....	9
	A. ATTITUDE DETERMINATION.....	9
	B. ATTITUDE CONTROL.....	10
	C. THERMAL CONTROL.....	12
	D. POWER SYSTEMS.....	13
	E. SENSING DEVICES.....	15
	F. COMPUTING AND ELECTRONICS.....	16
IV.	THE QUANTUM REVOLUTION.....	19
V.	QUANTUM DOT THEORY.....	21
	A. ELECTRON CONFINEMENT.....	21
	B. QUANTUM DEVICE FABRICATION.....	22
VI.	THE DEPLETION REGION	25
	A. DEPLETION REGION FUNDAMENTALS.....	25
	B. DEPLETION WIDTH FOR PLANAR SURFACES.....	26
	C. DEPLETION WIDTH FOR CYLINDRICAL SURFACES.....	28
VII.	RESULTS.....	31
	APPENDIX A. NANOSATELLITE LAUNCH VEHICLES.....	35
	APPENDIX B. CURRENT NANOSATELLITE PROJECTS.....	43
	LIST OF REFERENCES.....	49
	INITIAL DISTRIBUTION LIST.....	53

ACKNOWLEDGEMENT

The author would like to acknowledge and thank Professor Luscombe for his guidance, patience and support during the work in performing this analysis.

I. INTRODUCTION

Most modern day satellites have masses on the order of several thousand kilograms. With launch costs rising past ten thousand dollars per kilogram, there is little mystery behind the movement to shrink the size of spacecraft. But loss of capability is a prime concern when reducing a satellite's overall size. To offset this loss, many programs have been undertaken worldwide to develop smaller satellites with advanced components allowing for a minimal loss of functionality.

At first, there were miniature satellites with masses less than 500 kg which were often simply stripped down versions of their larger cousins. Next to develop were microsatellites, those having masses of around 100 kg, which employed advancing technologies but were again limited in the scope of their missions. Currently under development, along with continued development of both mini- and microsatellites, are nanosatellites; spacecraft with masses of approximately 10 kg. Early nanosatellites have suffered in functional capacity as did their predecessors; however, modern technology and advanced engineering techniques have allowed for small satellites and satellite components which are capable of performing a variety of missions.

Nearly every component subsystem of a spacecraft can be reduced in size through advances in a variety of technologies. Of these subsystems, computers and electronics play a vital role as the central nervous system of most satellites. Nanosatellite designs benefit from smaller scale electronics, giving them more on orbit processing and more autonomy at a fraction of the weight. Much of the progress in the microelectronics has come from the reduction of size of the transistors that make up the integrated circuits, devices whose size

has dropped by a factor of ten in the last decade. [Ref 1]

As microelectronic components approach geometries on the order of nanometers, a full understanding of the quantum properties of such a device becomes imperative. In such semiconductor structures, knowledge of the extent of depleted regions is a significant parameter in grasping device operation, the size of the depleted regions generally represents a small fraction of the device geometry. In nanostructures, however, the spatial extent of the depleted regions are often comparable to the physical dimensions of the device.

This thesis will show that the curved interface of certain nanoscale devices presents new challenges in the accurate determination of the depletion region. Also, if the standard formula for the depletion width of a planar interface is applied, it will generally underestimate that width. Accurate modeling is essential as small errors in the estimation of the depletion region can potentially represent a discernable fraction of the device geometry.

II. NANOSATELLITE APPLICATIONS

A. WHAT IS A NANOSATELLITE ?

After 40 years of evolution, conventional satellite technology is concentrating on relatively few large satellites with high reliability and extensive capabilities. In certain applications however, larger numbers of smaller satellites can provide a much lower cost alternative without undue risk. Since the early days of Sputnik and Explorer in the late 1950's, developers have built small, simple systems alongside large, more conventional satellites. Miniature satellites, those spacecraft less than 500 kg, were designed to fill certain niches which required a short mission duration with relatively few subscribers. These small satellites were assembled quickly by small teams, often with significant program risks. However, in most small satellite programs, accepting a mission failure was the only alternative to not attempting the mission at all. With less money at stake, users were more apt to take risks with newer unproven components and more liberal designs in hopes of validating of those technologies. [Ref 2]

In today's terms, the word nanosatellite generally refers to space vehicles with a mass of less than 10 kg with most being only a few centimeters in diameter. [Ref 3] Although only a few such craft are in developmental stages today, some of which are listed in Appendix B, many more will follow as their capabilities increase. The functionality of these satellites is completely mission dependent with some being fully autonomous and others much more simplified. In the earlier years, as was aforementioned, small satellites were possible only at

the expense of functionality. This is no longer the case, however, with the internal systems of modern nanosatellites being identical to their larger counterparts although with micro-miniaturized systems performing all of the necessary tasks.

B. ADVANTAGES OF NANOSATELLITES

1. Cost

A new trend is emerging in the satellite market with the theme of “smaller, cheaper, faster, better”. This trend is driven by many different factors: the need to lower up-front costs of satellite procurement and a need to lower the launch and overall operations cost. Current U.S. military satellites are too expensive to build and fly in an era of constricting budgets. According to James Stuart, the cost required to engineer, launch and operate a small, medium and large geosynchronous satellite are \$100, \$150 and \$275 million, respectively with launch costs generally dominating the budget. Payload and platform are the other two major contributors to the cost. The platform mass and cost are related to the payload mass, power requirements and volume. Thus any reduction in mass, volume or power consumption is highly desirable and will have a significant impact on cost. Nanosystems are considered an excellent means of obtaining these reductions. These types of systems could lead to decentralization, whereby a given number of dispersed components could be used in place of a larger centralized unit, therein achieving higher efficiency, better redundancy and eliminating single point modes of failure. This leads to cost reduction in space based systems not only at the platform and payload levels but also in the ground facilities and launch vehicles, a few of which are described in Appendix A, down to the end-user achieved through the economies of scale. [Ref 4]

2. Redundancy

But cost-savings through the reduction of mass is not the only desirable aspect of nanosatellites, redundancy being another key feature. As they are small, these satellites can be mass produced in an assembly line fashion, a technique which is impossible for larger satellites. Spacecraft manufacturing is currently a labor intensive artisanal process with few similar units ever being produced. Traditional cost-reduction methods such as new design and production paradigms, modularity and pre-fabrication have reduced overall costs but not to the desired levels. A sensible way to cut cost and enable commercialization could be through a technology or engineering breakthrough oriented towards mass production of space subsystems. [Ref 4] Bulk production of these smaller systems would also lead to the possibility of incorporating redundancy into the layout of individual components. In current satellite designs, mission critical subsystems are replicated in their entirety to avoid single points of failure, resulting in added weight and complexity. The small size of nanosatellite components alone allows for the duplication of most subsystems many times over without a noticeable increase in mass. Redundancy can also be achieved at the architecture level by using a low-earth orbit (LEO) constellation. An example might be an array of nanosatellites in random LEO orbits providing fully connected, continuous communications as shown in Figure 1. With random individual orbits, the satellites require no orbit maintenance and can be flown in tandem with any LEO launch. In a short time the network could become fully populated. [Ref 2] A computer model of this type of network has demonstrated that a network of 400 satellites could provide 95% global coverage. [Ref 2]

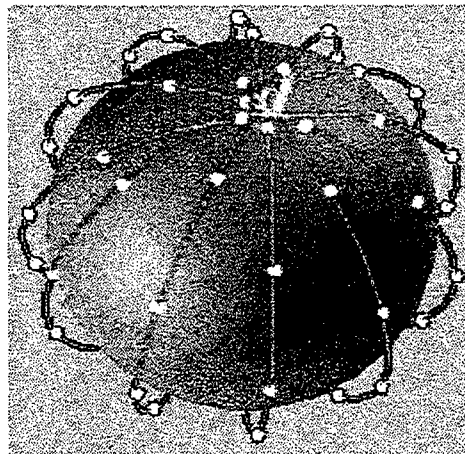


Figure 1 - Constellation of nanosatellites. From Ref. [5]

The intrinsic redundancy of this type of system is its inherent beauty. Destruction of 15 or 20 satellites has no effect on the overall system integrity and presumably the cost to destroy enough satellites to disrupt the network would cost more than the network itself. An added benefit is their small size which makes them nearly impossible to track.

3. Utility

Due to their reduced weight and volume, a small constellation of communication nanosatellites could be placed into orbit by a vast array of launch vehicles, quickly providing communications capability anywhere on the globe. Assuming a constellation of nanosatellites are preconfigured for contingency operations, these satellites could be stored in their launch vehicle and be lifted into space to support communications in regions with military operations, natural disasters or other emergency situations.

More often than not, military operations in remote areas of the world suffer in their initial stages primarily from a lack of dependable communications. When the U.S. began its build-up of forces in the Saudi Arabian desert prior to Desert Storm, demand for satellite communications outstripped the capability of military satellites in the area. As Air Force Brig.

Gen. William Jones, deputy chief of staff for requirements at the Air Force Space Command, said; "We found ourselves in a very tenuous position in the early days, until we could get satellite constellations optimized". [Ref 4]

III. NANOTECHNOLOGY IN SMALL SATELLITES

A. ATTITUDE DETERMINATION

Attitude sensors can be divided into two distinct groups: inertial and optical. Inertial sensors include such devices as accelerometers and gyros and have shown a theoretical performance dependence on the size of the instrument. The dimensions of optical sensors are determined by the diffraction-induced resolution limits of the optics. Efforts are currently underway to design nanosensing devices for both optical and inertial systems with the latter being more feasible albeit at considerable cost. Although there is substantial research in micro-earth sensors, sun-sensors and micromachined gyros, the most promising design is of a different sort.

A group at the Jet Propulsion Laboratory (JPL) has demonstrated a new sensing technique that involves combining micromachined silicon structures with a highly sensitive electron tunneling device. This device has an advantage of a reduction in the mass and volume of sensor/actuator systems by a factor of 100 to 10,000. These devices offer an improved sensitivity by a factor of 20,000 over that of conventional capacitive transducers and also require simpler electronics, less power and have dimensions of less than $10 \times 10 \mu\text{m}$. They experience no problems from differential thermal expansion, radiation effects or mechanical properties and can be mass-produced with standard lithographic techniques. The benefits of the electron-tunneling displacement sensors are extensive and include: greater sensitivity, reduced mass, smaller size, and immunity to the space environment. [Ref 6]

Another attempt to provide low-cost accurate attitude determination is the GPS Attitude Determination Flyer (GADFLY). Built by TRW and flown on the demonstration microsatellite "Lewis", GADFLY attempted to verify the accuracy of GPS based attitude determination. Similar experiments had flown previously but the Lewis experiment contains better filtering and processing of the GPS data with a more robust receiver that is less susceptible to solar radiation. [Ref 7]

B. ATTITUDE CONTROL

Although microsensors can be scaled irrespective of satellite size, the same cannot be said for the microactuators which physically control the motion of the spacecraft. It is feasible that, for applications that require low pointing accuracies, passive attitude control via scaled down gravity gradient booms or magnetotorquers could be employed. For missions with higher pointing accuracy requirements, i.e. +/- 2 degrees or those needing full 3-axis control, more advanced systems would be necessary.

Attitude control of three-axis stabilized spacecraft is accomplished by a variety of systems comprised of momentum wheels, reaction wheels or control moment gyros. There are two different classes of three-axis stabilization: momentum bias, which places a momentum wheel along the pitch axis and zero momentum systems which have a reaction wheel along each of three axes. It is well known that both stabilization methods can be accomplished by all thruster systems. On modern spacecraft, all thruster systems are usually not attempted because the constant drain of propellant makes for a poor satellite life expectancy. However, recent advances in Pulsed Plasma Thruster (PPT) systems promises to provide a simple, low mass, high specific impulse (I_{sp}) propulsion system which can be

effective in both attitude control and orbit maintenance.

The PPT is an electric propulsion device which uses electric power to ionize and electromagnetically accelerate a plasma to high exhaust velocities, attaining an I_{sp} in the 1000-2000 second range. [Ref 8] The PPT is ideal for small spacecraft since it has a low (0.1-50W) power draw, a small (50-800 μ N-s) impulse bit (Ibit), and uses an inert and inherently stable propellant, Teflon. The use of the Teflon as a propellant provides other advantages such as eliminating the need for expensive propellant feed systems, fuel heaters, tanks and valves. A comparison of minimum impulse bit characteristics is shown in Table 1 for several thrusters.

Thruster	Thrust (N)	Ibit (mN-s)
Monopropellant	0.448	5.34
Bipropellant	5.0	100
Cold Gas	0.05	0.5
PPT		< 0.1

Table 1 - Comparison of various impulse bits. From Ref. [8].

Although other electric propulsion devices such as resistojets, arcjets and ion thrusters are capable of an equally high I_{sp} they require much greater power than most small satellite buses can provide. Operational PPTs have proven effective with only 6-30 W and can be used as attitude controllers with an average power of less than 1 W. A flight test and evaluation of a PPT on orbit will be conducted by the Air Force's Phillip's Lab in mid 1999 when the second MightySat I satellite is scheduled for launch. [Ref 8] Table 2 gives a mass comparison of the PPT vs. more conventional attitude control systems used in the requirements analysis of a 100 kg LEO satellite. The only foreseeable sticking point to using the PPTs in nanoscale satellites is the capacitor technology. PPTs require a capacitor for

energy storage in order to deliver electrical power in short bursts. Expanding the energy density and lifetime of these capacitors while at the same time keeping their mass to a minimum is a concern. Currently, NASA's Lewis Research Center is working to reduce the mass of today's best PPT by one half. The goal is to develop a PPT which can

Component	Unit mass (kg)	No. of Units	Total Mass (kg)
Spinning mass	3.6	4	14.4
Drive electronics	0.91	4	3.64
Structure	2.0	1	2.0
System mass			20.04
Thruster dry mass	0.4	6	
280s I_{sp} propellant	3.73	N/A	
Six thruster mass			6.13

Table 2 - Mass of PPT vs. other thrust systems. From Ref. [9].

deliver 20 million pulses at a total energy level of 40 J and have a total system mass less than 1 kg. [Ref 10]

C. THERMAL CONTROL

Since nanosatellites are designed around a bus with relatively small dimensions, the removal of heat is greatly simplified. In fact, a nanosatellite can be thought of as isothermal, which facilitates the thermodynamic analysis and design process. An isothermal satellite which generates all of its power via body mounted solar panels, as most do, can be thermally controlled to within reasonable limits by the use of simple surface coatings and phase change materials. [Ref 11]

However, as the power requirements for more complex nanosatellites increase, it may be necessary to add deployable solar arrays or other energy sources. Consequently, the heat dissipation requirements will increase until there is not sufficient area on the nanosatellite's tiny frame to radiate the heat generated. The satellite will then require the use of miniature heat pipes, micromachined heat pumps, or deployable radiators to increase heat rejection and maintain operating temperatures.

At the forefront of nanosatellite thermal control is the development of mechanical cryorefrigerators and heat pumps based on a micromachining technology. These techniques have not yet been proven in nanosatellites and would not be the best approach for long term space missions as they require a steady flux of coolant gas. A closed loop version of the system is a possibility and could be used to cool the focal plane of a nanosatellite's infra-red (IR) system. Although miniaturized cryorefrigerators and heat pumps will take more than ten years to develop, an IR imager using microbolometers and operating at room temperature has already been demonstrated and may be the best hope. [Ref 11]

D. POWER SYSTEMS

To date, the power requirements in small satellites have been small enough for body mounted solar panels to be sufficient. Theoretically, solar cells can be reduced to any practical size with the only limitations being in the manufacturing processes of the cells themselves. Likewise, there is no fundamental obstacle to the furthered scaling down of batteries with modern technology employing a vast assortment of small batteries in pacemakers, watches and calculators. Advances have been made however, in more efficient solar cells for nanosatellites with smaller batteries as well.

The second MightySat I microsatellite will be the first to fly with dual junction solar cell technology. [Ref 12] These cells offer a 15% improvement in performance over conventional gallium-arsenide (GaAs) cells. The dual junction cells have a layer of gallium-indium-phosphide (GaInP) placed over a layer of GaAs. The GaInP absorbs shorter wavelength incident photons which would normally pass unhindered through a GaAs-only cell. The longer wavelength solar energy passes harmlessly through the GaInP and is absorbed by the GaAs. Combined, these layers provide electrical power at an efficiency, solar energy in divided by electrical power out, of 21% compared with conventional GaAs cells which realize an efficiency of around 18% and silicon cells which offer 14% efficiency. It remains to be seen what the degradation effects are on dual-junction cells over prolonged exposure to solar radiation but the design appears promising for now. [Ref 12]

Significant progress has also been made in the size reduction of spacecraft batteries which have been notorious as the greatest distributions of mass in many spacecraft. Although nickel-hydrogen (NiH₂) battery technology is not new, Eagle-Picher Industries (EPI), has developed a Dependent Pressure Vessel (DPV) design which combines the advantages of NiH₂ electrochemistry with the simplicity and extensive heritage of nickel-cadmium (NiCd) battery system. The 15 amp-hour cell design offers a 1.25 VDC output which will usually require the cells be wired in series as most applications require somewhat higher voltages. Each cell has a diameter of 5.5", a thickness of 1.12" and mass of 4.85 grams, thus offering a significant size and weight savings over more conventional designs. [Ref 13]

E. SENSING DEVICES

In the current generation of launch vehicles and spacecraft, temperature and pressure sensors are utilized mostly in housekeeping roles. Pressure sensors are mainly used for propellant tanks and lines while temperature sensors have a much wider range of applications. Thermal monitoring of a spacecraft is often accomplished with up to one hundred temperature sensors distributed throughout the body of the satellite. Examples of subsystems where one is likely to find temperature sensors include: solar arrays, propellant tanks, thruster components, heater controls on electronic components, payload components such as traveling wave tube amplifiers and cryogenic cooling systems. The current models of temperature sensors are thermistors and thermocouples both of which are solid state devices with masses substantially less than one gram. However, most of the mass associated with thermal sensors is packaging. Packaging is required for a variety of reasons, such as to protect against corrosive environments or simply to securely mount the sensor. Hence, decreasing the mass of the sensor itself is essentially useless while decreasing the mass of the packaging is virtually impossible. [Ref 8]

Pressure sensors, on the other hand, consist largely of piezoelectric crystals which usually have a mass of a few grams. Attempts are currently underway to fabricate pressure sensors from vapor-depositing piezoresistive films, whose electrical resistance changes as a function of pressure. These new sensors work well at room temperatures but present problems at temperatures below around 77K. [Ref 8]

In addition to piezoresistive films, piezoresistive elements are being made directly into silicon structures through ion implantation but also act in a non-linear fashion at cooler

temperatures. Another new technique is measurement via a fiber optic line. Essentially, a fiber optic wire is placed between two plates in such a way that the line will be bent as the plates are pushed together or pulled apart. As the fiber is bent, its optical properties will be altered in such a manner that can be measured and directly related to the pressure between the plates.

In most nanosatellites, experts agree that temperature and pressure sensors will be implanted directly into specific structures eliminating the use of packaging. Due to their small size, the number of sensors which a spacecraft can support will be largely determined by the amount of data the satellites computer can handle. [Ref 8]

F. COMPUTING AND ELECTRONICS

Though not usually a mass or volume constraint, reduction in the size of onboard computing electronics with a marked increase in computing power would have a significant impact in spacecraft functionality especially in the area of deep space missions. The Center for Integrated Space Microsystems (CISM), the advanced computing department at JPL, has recently been directed by NASA to advance the state of the art in microelectronics for near- and mid-term missions. The CISM is actually one element of a larger NASA program termed X-2000 which aims to produce a standardized spacecraft bus which can be tailored to various mission requirements. But CISM officials have been challenged to design long-term revolutionary computing technologies smaller than the width of a human hair. Eventually, these technologies, based on the use of the innovative quantum dot, will be used to improve U.S. encryption of national security transmissions. According to its director, Leon Alkalai, "We (CISM) are studying how to build devices at the atomic or molecular scale, also referred

to as molecular nanotechnology". [Ref 14] Miniaturizing "electronics down to where everything is dealing with electrons and photons" will allow NASA and other national agencies to construct intelligent and fully autonomous systems on a microchip for use in rovers, orbiters and other space systems, Alkalai said. [Ref 14]

Most of today's satellites contain classical computer systems in which all computing logic is determined by switches between one and zero. In future "quantum computers" decisions are based on energy levels of electrons allowing for an incredibly reduced size of scale.

While security agencies are fascinated by the capabilities of quantum computing and its ability to keep messages secure, NASA is interested in building a quantum computer "because it would be a breakthrough technology equivalent to the development of the transistor 50 years ago" Alkali said. Both British and Japanese agencies have approached CISM in an effort to jointly explore quantum computing for use in deep space nanosatellites and other applications. [Ref 14]

By the year 2010, it is hypothesized that many important NASA missions will require computing power approaching one petaflops (10^{15} floating point operations per second). Unfortunately, it is uncertain whether or not the U.S. computer industry alone can fill that need at an acceptable cost. To achieve such a high level of performance, significant breakthroughs in computing hardware technologies, i.e. the quantum computer, must be realized. [Ref 14]

IV. QUANTUM REVOLUTION

Nanosatellites are but one of a myriad of beneficiaries of quantum computing technologies. Integrated circuits have become the technology of choice for electronic functions. Their use has become so widespread that they dominate the world electronic markets and have opened new markets which were previously nonexistent. As the demand for these semiconductor devices has increased, so has their size decreased. According to Moore's Law, the number of transistors on a single integrated circuit chip should continue to double each year. But doubling the number of devices on a chip requires reductions in both the size of the devices themselves and their interconnections. As the size of current chip designs dip below 0.25 micrometers, one must wonder as to the eventual limit of the ever-shrinking transistor. [Ref 15]

It was thought in the mid-1980's that further size reduction of electronic devices below the micrometer range would yield diminishing returns. However, newly developed quantum dots have been fabricated at a width of only 100 nm. [Ref 15]

In this regime, the fundamental quantum properties of a single electron will dominate charge transport and also, at these dimensions, it is no longer satisfactory to think of electrons as particles. It has been determined from such phenomenon as diffraction that electrons have properties consistent with a wave nature which are described by the electron's wave function. By exploiting this wave function, we can harness the electron's ability to tunnel through a potential energy barrier, rather than having to go over it as a classical particle would. This situation is known as resonant electron tunneling and is used in the simplest practical

nanoelectronic device; the resonant tunneling diode (RTD). [Ref 16]

In an RTD an electron is quantum-mechanically confined in one direction and is otherwise free to move in the remaining two directions. This confinement produces a nonlinear device characteristic that has innovative circuit applications. [Ref 16]

But the quantum dot achieves three dimensional electron confinement which is the inevitable result of continued downscaling of semiconductor structures. The quantum dot probably represents the smallest possible noncryogenic switching device and perhaps reaches the ultimate scaling limits of solid state electronics.

[Ref 16]

V. QUANTUM DOT THEORY

A. ELECTRON CONFINEMENT

Technological advances in semiconductor materials science and photolithography continue to force the size of the transistors that make up integrated circuits to smaller and smaller limits. Device geometries on the order of 350 nanometers are now being constructed in mass quantities, launching us into the new realm of nanotechnologies at the forefront of which is the quantum dot.

The ability to confine an electron to a given point has proven elusive. Scientists had, for some time, been able to reduce the electron's dimensions to lines or planes but have recently confined it in all three spatial dimensions; hence a dot. Physicists have developed new methods for artificially "creating" atoms, no longer relying on the natural solid state structure of atoms, molecules, and crystals. These so called "designer atoms" have recently proliferated and their capacities are as yet untapped. [Ref 17]

Applications of quantum dots to the fields of optics and micro technologies are virtually without bounds. Materials may be fabricated which are capable of resonating at any frequency chosen by the designer, giving rise to very precisely tuned semiconductor lasers and other applications such as arrays of densely packed quantum dots molded into a substrate and used as transistors for more powerful computing.

Quantum wells were the first successes in two-dimensional fabrication. These structures, made by thin film epitaxial techniques, grew a semiconductor structure as a series of individual layers, each comprised of semiconducting material (usually gallium arsenide,

GaAs, and related compounds). [Ref 17] Since electrons tend toward states with the lowest energy possible, and the energy of electrons inside the well are relatively lower than those outside, electrons are forced into the well. Quantum wells are ubiquitous. No longer relegated to simple constructs in quantum physics textbooks, they appear in laser diodes which drive our compact disc players and are found in communications electronics such as microwave receivers. [Ref 18]

B. QUANTUM DEVICE FABRICATION

Fabrication of nanoscale structures has proven difficult. The first attempts made use of nanocrystallites, crystals which, when formed with glass at high temperature precipitate in the glass, forcing electrons into a state of quantum confinement. It is important to note that when particles are confined to a certain space, the boundary conditions and wave properties of the particle dictate that the particle may occupy only certain discrete values of energy. While strict 3D confinement would yield truly discrete energy levels, the electrons would also be inaccessible for transport. Thus, it is necessary in quantum dot structures for the dot states to be slightly unbound in one or more dimensions. Nanocrystallites have chemical properties which dampen the vibration of electrons at higher energies, and thus a quantum dot made of nanocrystallites could only operate at unsuitably low energies. [Ref 17]

The manufacturing process usually begins with molecular beam epitaxy (MBE) onto a stable substrate. An MBE system is simply a very high vacuum evaporator. By rigidly controlling the temperature of the single crystal substrate and flow rate of the evaporated molecules, it is possible to achieve high purity epitaxial growth. Figure 2 shows an example of an MBE system. As the crystal is grown, the effusion cell shutters are opened and closed

as necessary, producing the desired layering. The result is either a heterojunction or a multi-

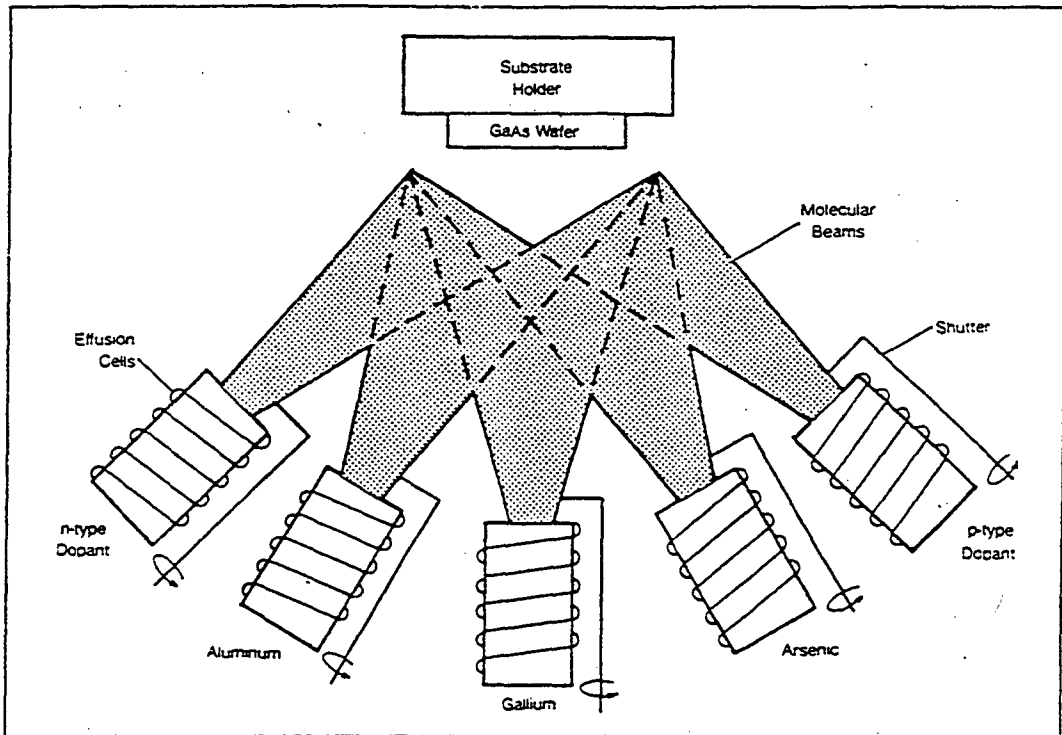


Figure 2 - Schematic of a molecular beam epitaxy system (MBE). From Ref. [18].

layered heterostructure. Once grown, the slabs of quantum well material are cut and etched by photolithography into semi-cylindrical pillars 100 angstroms wide as shown in Figure 3. Quantum dots of different sizes have different sets of harmonic energy levels, a clear signal that the electron is indeed confined. Various research has shown it plausible to construct a potential gate around the dot which squeezes it, thus increasing its spectrum of energy levels. The squeezing is accomplished by making the conducting strips around the electron negatively charged so that the electrons in the quantum well beneath the surface will be repelled. However, since the electrons are confined to a thin layer parallel to the surface, the lateral direction is the only allowed dimension for movement. As a result, the electrons are confined to a tiny cluster directly underneath the central square outlined by the electrodes. As the

square is reduced in size, a quantum dot is formed. This electrostatic squeezing has proven to be the most successful method of controlling the size of individual dots. The problem that arises is the difficulty in manufacturing electrical contacts small enough to allow for resonant tunneling in and out of the squeezed dot. Recently however, successes have been realized in the assembly of miniature tunnel barriers who are themselves electrostatically controlled.

[Ref 17]

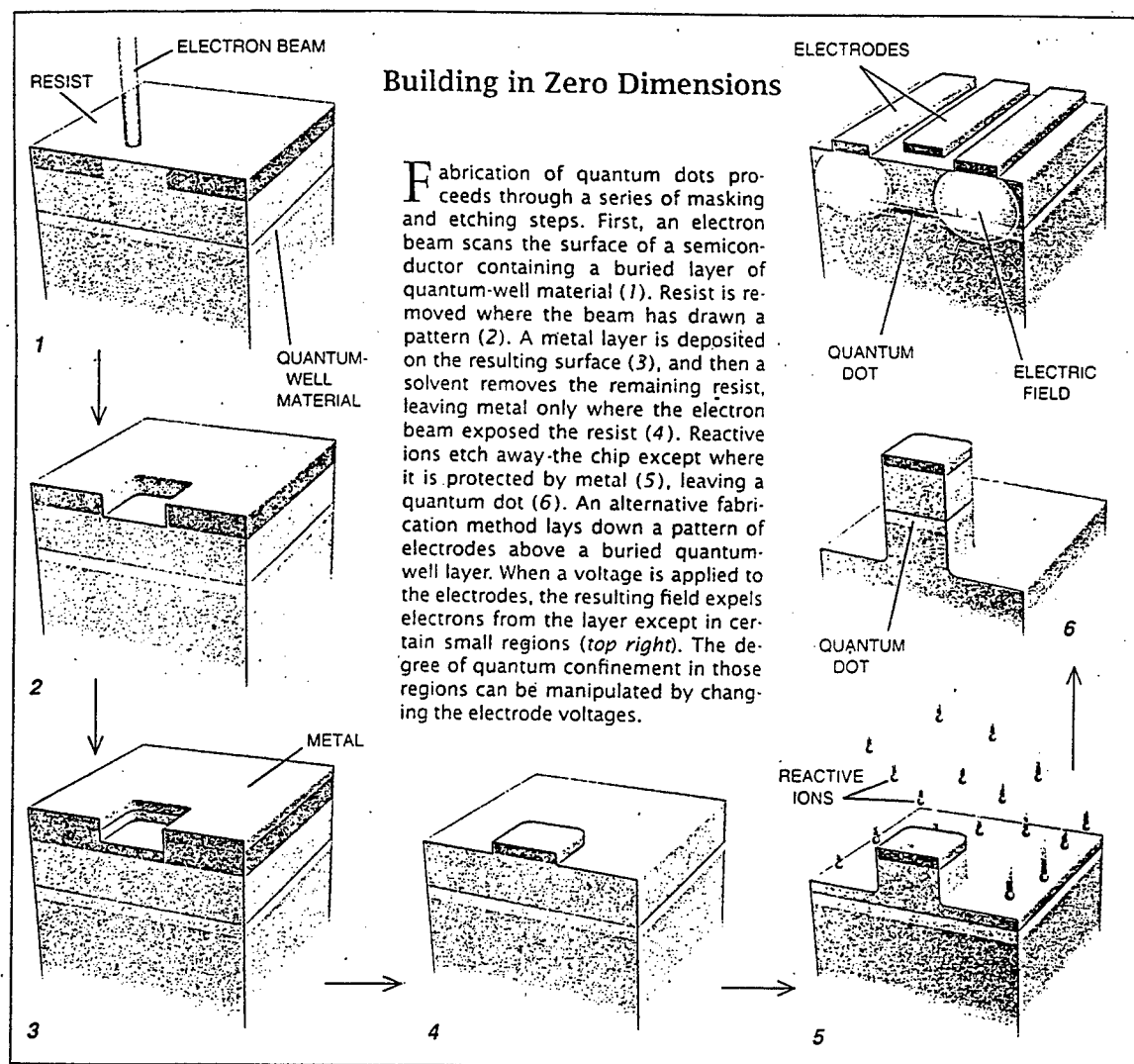


Figure 3 - Etching of quantum dots. From Ref [17]

VI. THE DEPLETION REGION

A. DEPLETION REGION FUNDAMENTALS

At the creation of a typical p-n junction there will be a motion of majority charge carriers across the junction. Electrons close to the junction plane will tend to diffuse across into the p-doped material leaving behind the donor sites fixed in the lattice and thereby creating a net positive charge on the n-type material. Upon reaching the other side of the barrier, the electron quickly drops out of the conduction band into the valence band and in a sense, combines with a hole. The holes experience a similar sequence when drifting across the junction from the p-type material to the n-type material. This motion of charges is the diffusion current. [Ref 19] In the steady state, a region of fixed positive charge builds up on one side of the barrier and a region of fixed negative charge builds up on the other side as shown in Figure 4.

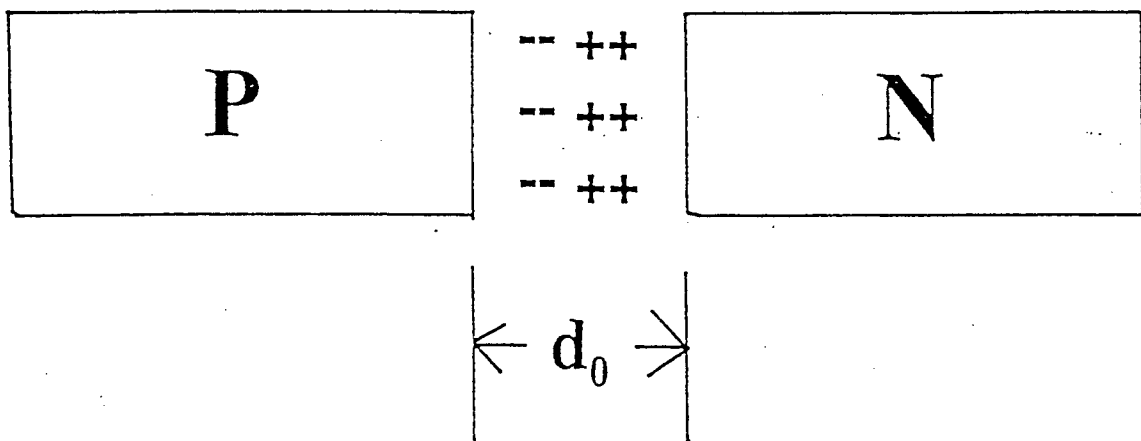


Figure 4 - Creation of a depletion region.

These two regions form the depletion region of width d_0 . The charges in the depletion region set up a potential barrier, as illustrated in Figure 5, against further diffusion by the majority

carriers but enhances movement of the minority carriers on both sides of the junction.

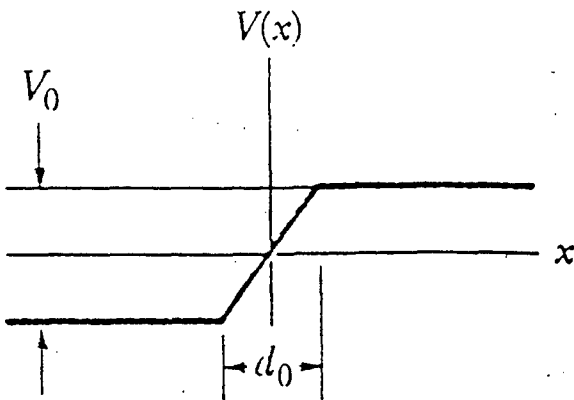


Figure 5 - Potential barrier at the depletion region. From Ref. [19].

When, by thermal agitation, an electron close to the junction plane has its energy increased enough to leap to the conduction band in the p-type material, the potential difference at the junction enables it to drift back the n-type material and likewise for the holes. This is the drift current and directly opposes the diffusion current in steady state analysis. This gives rise to the term "depletion region" as that area in proximity to the junction is swept free of charge carriers. [Ref 19]

B. DEPLETION WIDTH FOR PLANAR SURFACES

In the depletion region, Poisson's equation can be written for the electrostatic potential ψ in the single 'x' dimension as

$$d^2\psi/dx^2 = qN_A/\epsilon_s \text{ for } -x_p \leq x < 0 \quad (1)$$

and

$$d^2\psi/dx^2 = qN_A/\epsilon_s \text{ for } 0 < x \leq x_n \quad (2)$$

where x_p and x_n are the lateral cutoffs for the neutral p-type and n-type regions respectively, ϵ_s is the permeability constant, q is the unit of charge and N_A is the number density of

acceptors and N_D is the number density of donors as shown in Figure 6. Since the semiconductor is overall electrically neutral, the charge density per unit area on the p-side exactly equal the charge density on the n-side:

$$N_A x_p = N_D x_n \quad (3)$$

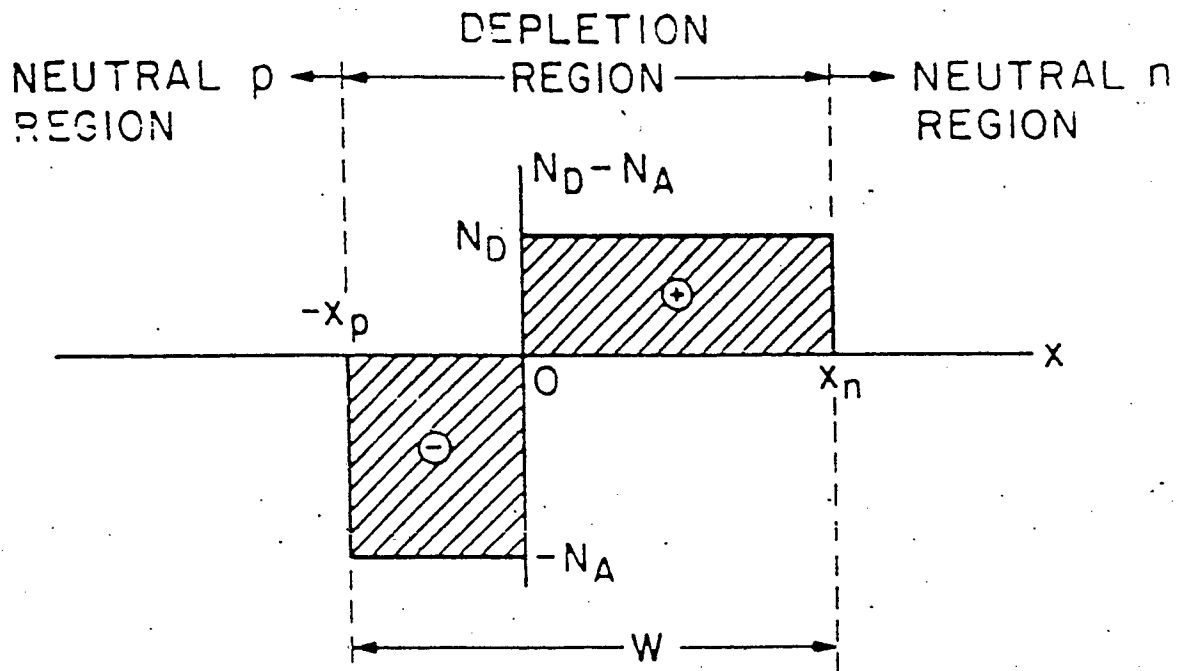


Figure 6 - Space charge distribution in the depletion region. From Ref. [20]

The width of the depletion layer W , is given by

$$W = |x_p| + x_n \quad (4)$$

Since the component of the electric field \mathcal{E}_x is the negative rate of change of the potential in the direction x , it can be found by integrating Equations 1 and 2 to yield

$$\mathcal{E}(x) = -\partial\psi/\partial x = -[qN_A(x + x_p)]/\epsilon_s \text{ for } -x_p \leq x < 0 \quad (5)$$

and

$$\mathcal{E}(x) = -\mathcal{E}_m + qN_D x/\epsilon_s = [qN_D/\epsilon_s](x - x_n) \text{ for } 0 < x \leq x_n \quad (6)$$

where \mathcal{E}_m is the maximum electric field which exists at the junction ($x = 0$) and is given by

$$\mathcal{E}_m = qN_D x_n / \epsilon_s = qN_A x_p / \epsilon_s. \quad (7)$$

To determine the potential, ψ_D , which occurs across the depletion region, we integrate Equations 5 and 6 to find

$$\psi_D = qN_A x_p^2 / 2\epsilon_s + qN_D x_n^2 / 2\epsilon_s = \mathcal{E}_m W / 2 \quad (8)$$

By combining equations 3 and 8 we obtain an expression for the width of the depletion region as a function of ψ_D

$$W = [(2\epsilon_s/q) \{ (N_A + N_D) / N_A N_D \} \psi_D]^{1/2}. \quad (9)$$

C. DEPLETION WIDTH FOR CYLINDRICAL SURFACES

Although Equation 9 is a sufficient approximation of depletion width at a planar interface, it is not satisfactory for a cylindrical geometry. For shorthand purposes, define a characteristic length, ξ , given in terms of Φ , the energy at any given surface within the semiconductor as

$$\xi = [\epsilon_s \Phi / e^2 N_D]^{1/2}. \quad (10)$$

Now, using cylindrical coordinates, Poisson's equation for an axisymmetrical potential, $\psi(r)$, can be written

$$\nabla^2 \psi(r) = (1/r)(d/dr)[r d\psi/dr] = \Phi / \xi^2 \quad (11)$$

where r denotes the radial position for cylindrical coordinates. The general solution to Equation 11 is

$$\psi(r) = \Phi[\gamma + \delta \ln(r/\xi) + 1/4(r/\xi)^2], \quad (12)$$

where γ and δ are arbitrary constants. In order to solve this equation, we must first impose some boundary conditions.

Between the neutral region and the depletion region on both sides of the junction is

a transition region as shown in Figure 7 for a planar geometry. Here the space charge of impurity ions, fixed in their lattice sites, are partially compensated by the mobile carriers. The transition region is very small on a scale with the depletion region and leads to the approximation that it can be neglected and the depletion region can be represented as a rectangular distribution shown in Figure 8.

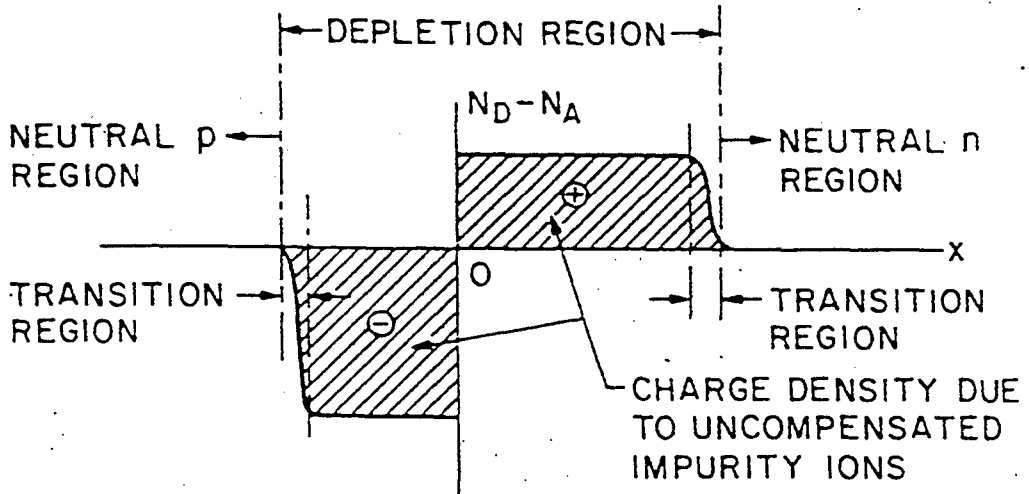


Figure 7 - Space charge distribution. From Ref. [20]

The assumption reveals that the potential, ψ , has zero slope at the interior edge of the depletion region, or

$$\psi'(R-W) = 0 \quad (13)$$

In addition to the interfacial boundary condition given as the definition of Φ , we also require that at an interior position $x = R-W$, ψ vanishes relative to E_F , the Fermi level energy, thus

$$\psi(R-W) = 0. \quad (14)$$

Imposing these boundary conditions on Equation 12 we obtain the transcendental equation

$$\Delta^2 = (R^2 - 4\xi^2) / (1 + 2\ln(R/\Delta)), \quad (15)$$

where $\Delta \equiv R-W$. For any given cylindrical geometry of characteristic length ξ and radius R ,

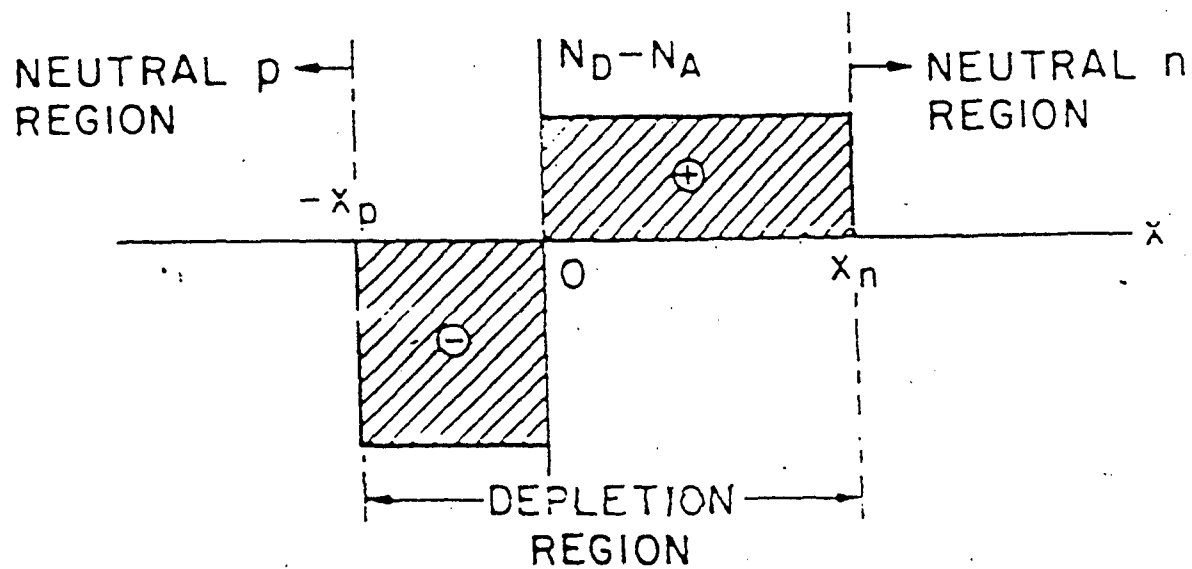


Figure 8 - Rectangular approximation of charge distribution. From Ref [20]

Equation 15 can be solved numerically for Δ . The width of the depletion region W , as illustrated in Figure 9, is now defined in terms of R as

$$W = R - \Delta. \quad (16)$$

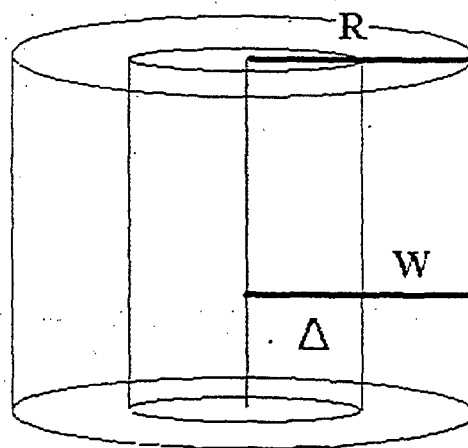


Figure 9 - Geometric Depiction of W .

VII. RESULTS

In solving Equation 15, it is convenient to simplify it by dividing through by R^2 and rewriting the denominator to obtain

$$(\Delta/R)^2 = (1 - 4(\xi/R)^2)/(1 - \ln(\Delta/R)^2). \quad (17)$$

Now we define two variables, namely 'x' and 'y' where $x = 4(\xi/R)^2$ and $y = (\Delta/R)^2$. This reveals an equation in y and x where $y = y(x)$ and both are dependent on the inverse of R^2 as

$$y = (1 - x)/(1 - \ln(y)). \quad (18)$$

It is apparent from the definition of x that it contains all of the relevant parameters of a given structure. In solving Equation 18 then, one could tabulate all corresponding values of y and leave only the structure radius R as the remaining factor. One would then only need to multiply by R to get Δ . A numerical plot of Equation 18, shown in Figure 10, shows that there are actually two solutions depending on whether y is less than or greater than one.

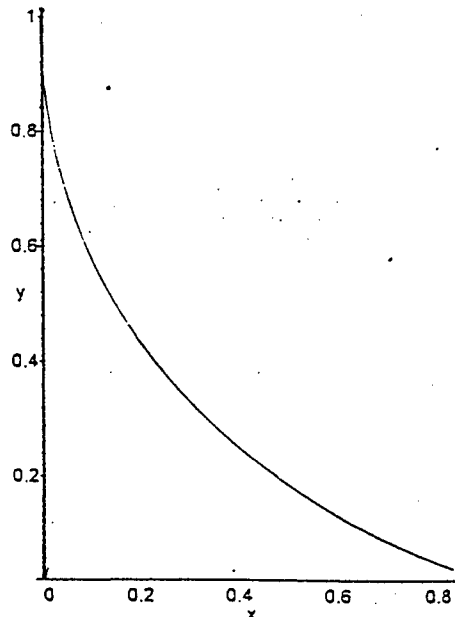


Figure 10 - A plot of y as a function of x.

But for $y > 1$, the definition of y demands $\Delta > R$ which is physically unrealizable. At the point where $y = 1$ we have $\Delta = R$ and Equation 18 gives

$$1 = (1 - x)/(1 - \ln(1)). \quad (19)$$

Simplification shows $x = 0$ or in more specific terms $4(\xi/\Delta)^2 = 0$. For this to be true either $\Delta \rightarrow \infty$ or $\xi = 0$. But Δ must equal R for $y = 1$ thus determining $\xi = 0$. We will again define ξ here as

$$\xi^2 = (\Phi \epsilon_r) / (e^2 N_D) \quad (20)$$

to illustrate that for $\xi = 0$, the dopant density N_D must become large. Indeed for highly doped structures of semiconductor material it is possible to inject dopants to the point where the entire structure is devoid of charge carriers, i.e. $\Delta = R$.

Further analysis around the point $y = 1$ can be made by saying as $R \rightarrow \infty$, $x \rightarrow 0$, thus $\{\Delta(R)/R\} \rightarrow 1$ giving $y \rightarrow 1$. We now let $y = 1 + \lambda$ where λ is a small term to be found. Substituting into Equation 18 yields

$$1 + \lambda = (1 - x)/(1 - \ln[1 + \lambda]) \quad (21)$$

Using the approximation of $\ln(1 + \alpha) = \alpha$ for any sufficiently small number α we arrive at

$$\lambda = \pm x^{1/2}. \quad (22)$$

Indeed, an expansion about the point $y = 1$, as shown in Figure 11 yields a parabolic curve as expected. The values of x were chosen as actual results given a GaAs structure with $\Phi = 0.7$ eV, $N_D = 10^{18} \text{ cm}^{-3}$, $\epsilon = 13.2\epsilon_0$ and a radius of 100 nm. These values yielded a value of $x \approx 10^{-5}$. A detailed analysis of x as $x(R, N_D)$ shows that as R is reduced by a factor of ten, x increases by a factor of 100. Likewise as N_D is reduced by a factor of ten, x increases only by a factor of ten. Thus, our expected values of x in a given semiconductor structure are

approximately bounded roughly by $10^{-5} < x < 10^{-2}$.

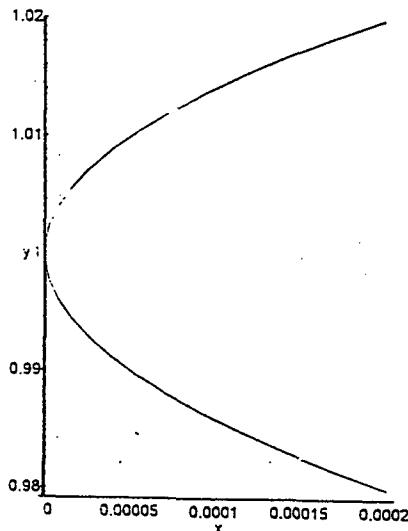


Figure 11 - Plot of y vs. x near $y = 1$.

Another point to be examined in the limit of W as $R \rightarrow \infty$ which should yield the same result as that for a planar surface. By substituting $\Delta = R - W$ into Equation 15, then dividing through by R it can be shown that

$$(1 - W/R)^2(1 - 2\ln(1 - W/R)) = 1 - 4\xi^2/R^2. \quad (23)$$

Again using the approximation for $\ln(1 + \alpha)$ and keeping the first two terms of the approximation we find

$$(1 - W/R)^2(1 + 2W/R + (W/R)^2) = 1 - 4\xi^2/R^2. \quad (24)$$

Expanding the left side of Equation 24 as a Taylor series gives

$$(W/R)^2(1 - W/3R) = 2\xi^2/R^2. \quad (25)$$

Clearing common terms from both sides of Equation 25 and defining a new variable W_1 we can say

$$W^2(1 - W/3R) = 2\xi^2 = W_1^2 \quad (26)$$

A clever guess at the value of W can be made by saying $W = W_1 + \beta/R$ where β is some

number to be determined. Analysis of Equation 26 shows that $\beta = W_1^2/6$ giving a result of

$$W = W_1(1 + W_1/6R + \dots)^2. \quad (27)$$

If $R \gg W_1$, then Equation 9 will suffice as an approximation to the depletion layer width. For materials such as GaAs and others whose doping densities are on the order of 10^{18} cm^{-3} , we see that W_1 is on the scale of less than 100 nanometers. Devices of this radii are currently in development and will benefit from the correction terms in Equation 15. Secondly, since the value of ξ is relatively fixed for a given material, it has been shown that the structure will be completely devoid of carriers as W approaches R ; i.e. the device is made smaller. Alternatively, for a fixed R if either the doping density is decreased or Φ is increased, again W will approach R .

In summary, this thesis has shown there is a more accurate method by which to describe the depletion width of a semi-cylindrical nanoscale structure such as the quantum dot. Applying the standard textbook formula for a planar interface has been shown to be inadequate. Future research into the possible graphical analysis of the equations presented would aid in the more thorough understanding of the geometrical picture at hand. If these devices do indeed represent the future of nanoelectronics as this thesis has claimed, a thorough understanding of the properties of nanostructures is imperative.

APPENDIX A. NANOSATELLITE LAUNCH VEHICLES

A. PEGASUS

The Pegasus is an air launched booster which uses three solid-rocket motors for propulsion and wings for lift. It is launched from the belly of a B-52 which enables it to achieve an orbit of any desired inclination. An inertial system guides the booster while aerodynamic fins control the first stage and vectorable nozzles assist the second and third stages. Figure A-1 shows Pegasus stages 1-3. [Ref 21]

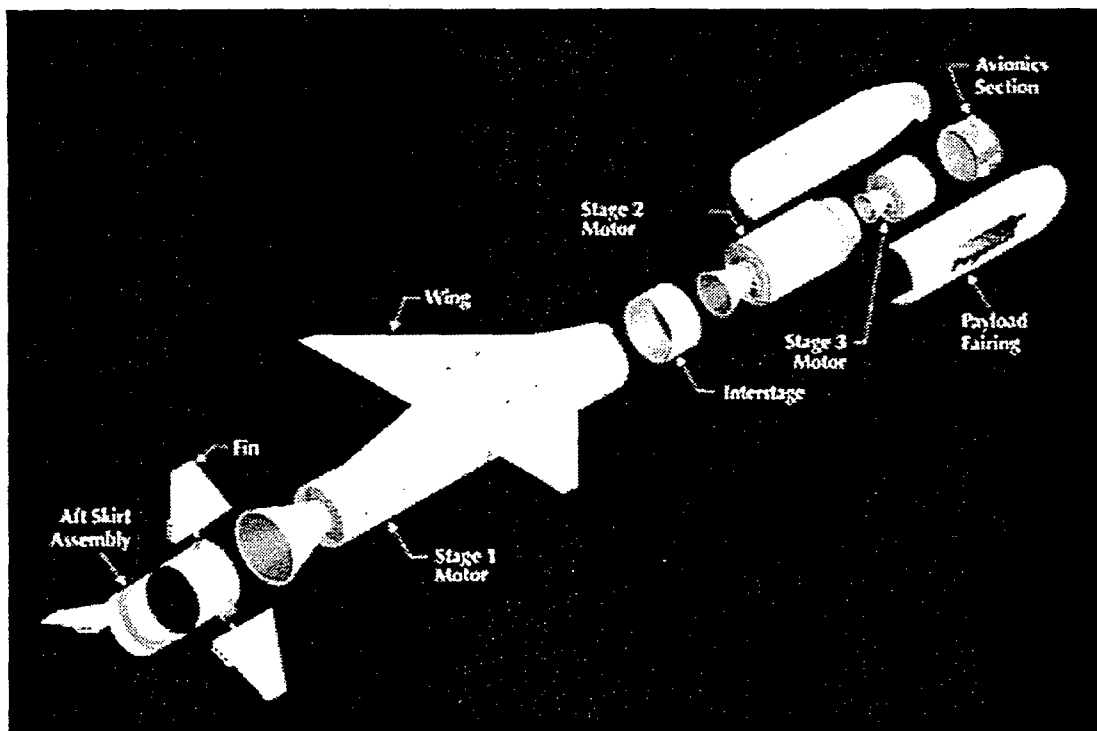


Figure A-1 - Pegasus launch vehicle. From Ref. [22].

The Pegasus orbit and payload capabilities are as follows:

- maximum payload weight
- 267 kg (250 nm polar orbit)
- 400 kg (250 nm equatorial orbit)

B. TAURUS

The Taurus XL expendable launch vehicle, pictured in Figure A-2, is the latest launch platform designed by the Orbital Sciences Corporation. It is essentially a Peacekeeper missile body with enough flexibility and transportability to allow its launch from any unimproved concrete pad. Like the Pegasus, it is an excellent platform for launching small payloads. [Ref 21]

Taurus payload and orbit statistics:

- 1390 kg (250 nm equatorial orbit)
- 450 kg (geosynchronous transfer orbit)
- 1180 kg (250 nm polar orbit)

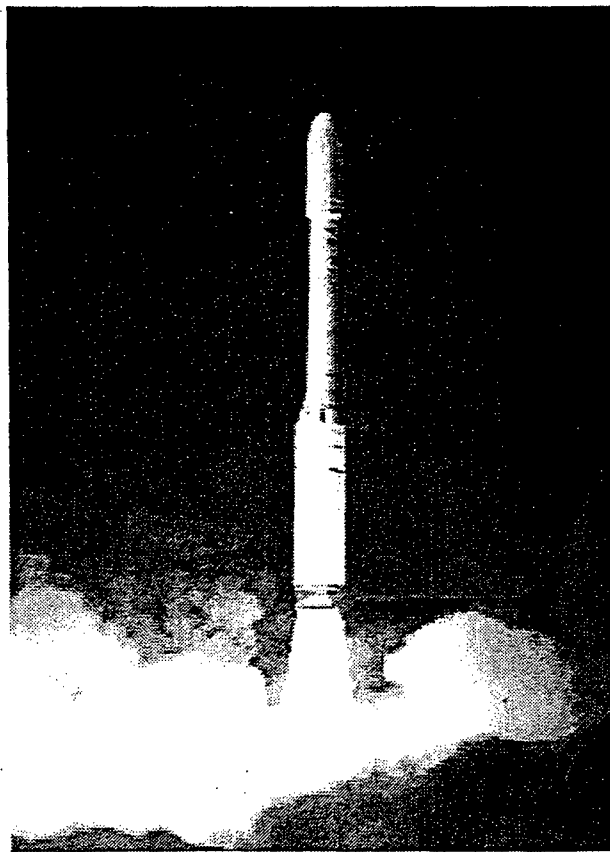


Figure A-2 -Launch of a Taurus rocket. From Ref [23].

C. SCOUT (ENHANCED)

The Scout launch vehicle, the first U.S. launch vehicle to use solid fuel exclusively, was designed by LTV as a booster for DOD and NASA and foreign space probes. The current Scout is a four stage solid propellant vehicle with maximum lift capabilities of up to 600 lbs depending on launch site and mission. [Ref 21] Figure A-3 shows a Scout launch from Vandenberg AFB.

Orbit and payload data for the Scout:

- 372 kg (100 nm polar orbit)
- 525 kg (100 nm equatorial orbit)
- 455 kg (100 nm @ 40° inclination)

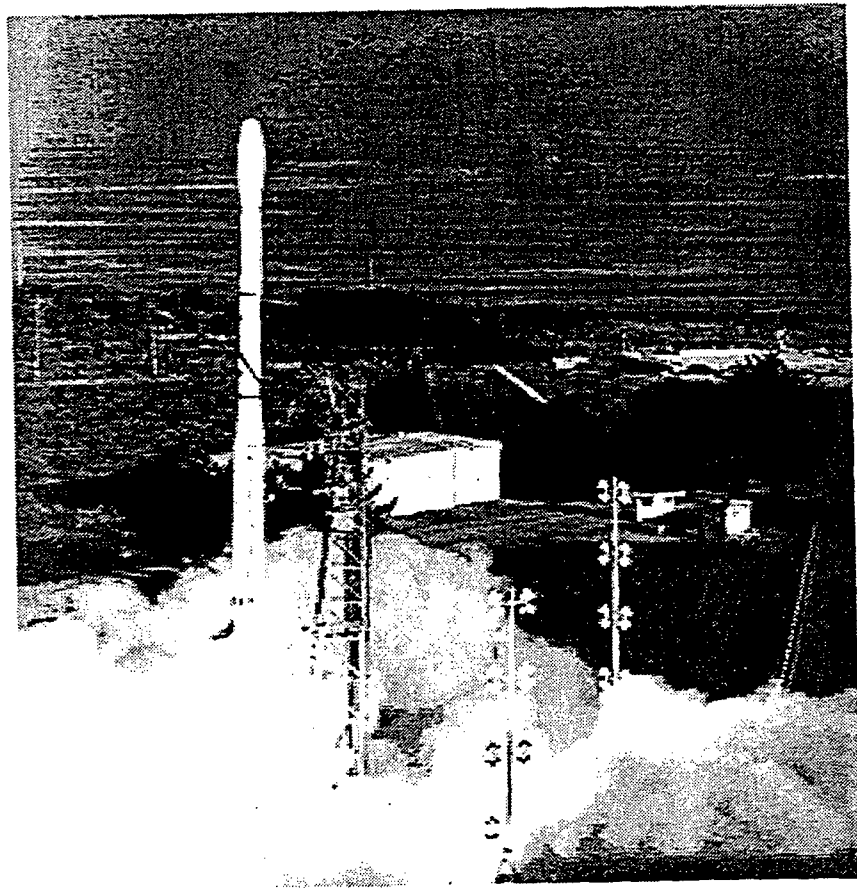


Figure A-3 - Scout launch from Vandenberg, CA. From Ref. [24].

D. TITAN II

The Titan II launch vehicles are decommissioned ICBMs that have been refurbished and equipped with hardware required for space launch. The Titan II is the smallest of the Titan series and has been modified by DOD for launches of smaller payloads into polar orbits. Figure A-4 shows a launch of the Titan II launch vehicle. The lift capacity for the Titan II varies from 1905 kg to 3720 kg depending on the number of strap-on engines required.[Ref 21]

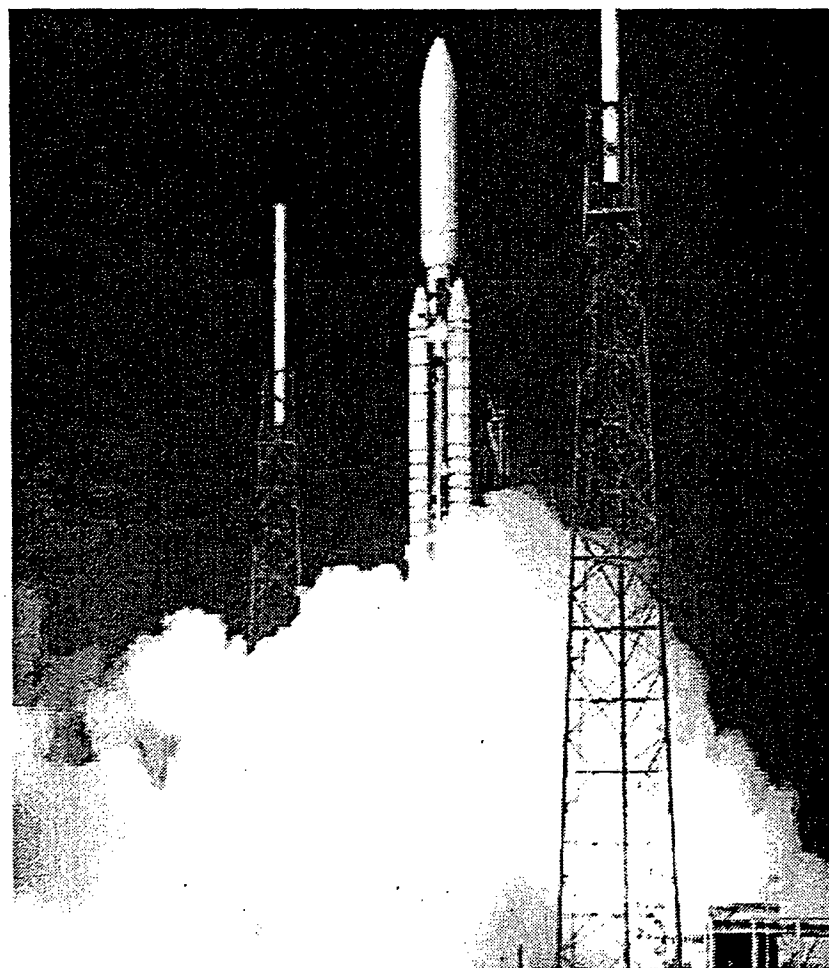


Figure A-4 - Launch of Titan II vehicle. From Ref. [25].

E. DELTA II

The Delta II is the newest, most powerful version of the Delta series originally developed by NASA in 1960. Since that time, the Delta rocket, shown in Figure A-5 launching Iridium satellites, has an average utilization of one launch every 60 days, a launch rate unmatched by any other platform. The Delta II is a three stage rocket with solid propellant for the first stage and liquid propellant for the last two stages. It's design tailors the rocket toward putting very heavy payloads into very high orbits but could also be used to lift many nanosatellites at once. [Ref 21] Specifications on the Delta II are as follows:

- 1885 kg (geosynchronous transfer orbit)
- 4000 kg (100 nm polar orbit)

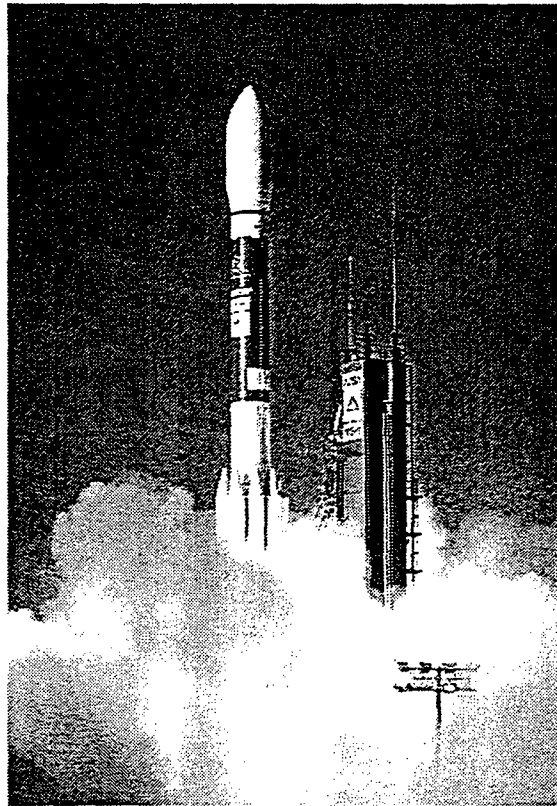


Figure A-5 - Launch of a Delta II. From Ref. [26].

F. SPACE SHUTTLE

The infamous Space Shuttle, shown in Figure A-6, was originally conceived in 1969 and consists of a delta winged orbiter, two solid propellant rocket boosters, which are both recoverable, and an expendable liquid fuel tank. The current method for launching nanosatellite-size craft from the Space Shuttle is the Get-Away Special (GAS) canister. These canisters are approximately the same size as a large trash can, are mounted in the orbiter's cargo bay and release their payload via a spring mechanism.

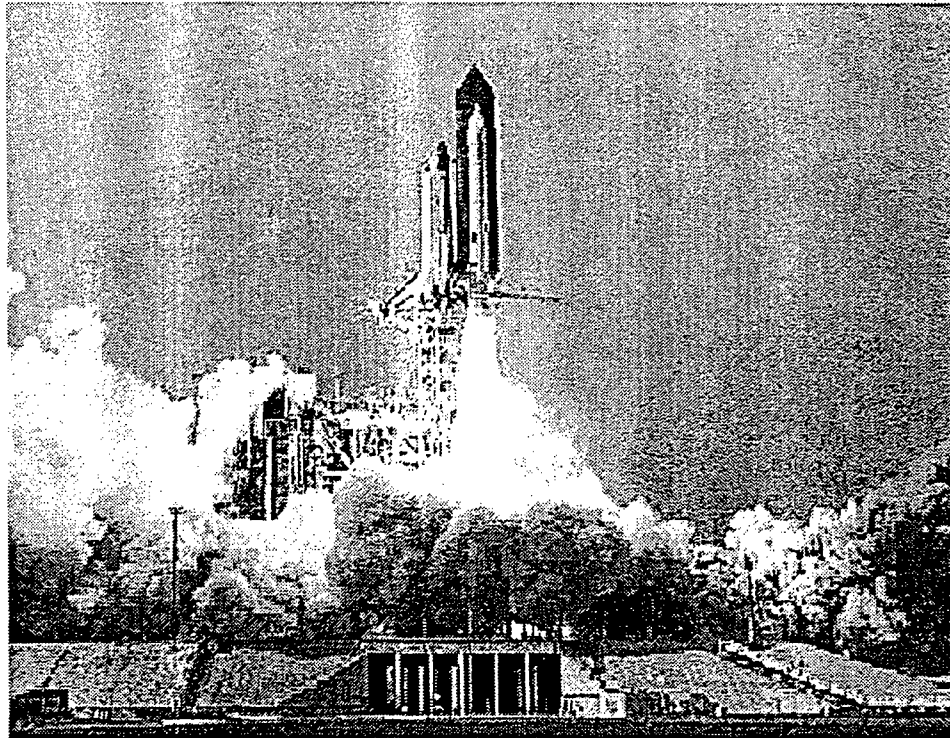


Figure A-6 - Launch of the Space Shuttle from Cape Canaveral. From Ref [27].

Standard and large are the two available sizes of GAS canisters. If the Space Shuttle were configured to solely launch nanosatellites, a bridge of twelve canisters could be constructed

in the main cargo bay or the nanosatellites could be mounted to a steerable sled which could be launched from the orbiter then maneuvered to launch each nanosatellite individually.

Space Shuttle payload characteristics are:

- maximum payload weight
 - 13608 kg (300 nm @ 28.1° inclination)
 - 8165 kg (300 nm @ 57° inclination)
 - 1361 kg (260 nm @ 98° inclination)

- payload bay dimensions
 - diameter: 15 feet
 - length: 60 feet

G. COMPARISON OF VEHICLES

Table A-1 below illustrates the differences among the various aforementioned launch vehicles in terms of their size and cost.

Launch Vehicle	Height/Length	Mass (lb)	Success Rate	Cost per Launch (98\$)
Pegasus	51 ft.	42,000	100 %	17M
Taurus	90 ft	180,000	100 %	17M
Scout	75 ft	109,000	87.6 %	15M
Titan II	140 ft	340,000	93 %	60M
Delta II	125 ft	506,000	94 %	60M
Space Shuttle	184 ft	4,500,000	97.4 %	150M

Table A-1 - Comparison of nanosatellite launch vehicles. From Ref. [21].

APPENDIX B. CURRENT NANOSATELLITE PROJECTS

A. GENERAL

There are currently a multitude of nanosatellite designs from around the world which are in various stages of design and deployment. Below is a partial list of these satellites which will be briefly described in this appendix:

- Munin
- Bitsy
- ASUSat I
- TUBSAT series
- SNAP-1

B. MUNIN

The Munin project is run by the Kiruna Division of the Swedish Institute of Space Physics and was originally conceived in September of 1996. The scientific objective of Munin is to collect data on the auroral activity on both the northern and southern hemispheres with a miniature CCD camera such that a current picture of the global state of activity can be made available via the Internet. The Munin nanosatellite will have a mass of approximately 5 kg and will have a cubic shape as depicted in Figure B-1. [Ref 3] Onboard it will house a combined ion and electron spectrometer and will also analyze high energy particles with a solid state detector. The spacecraft has a passive attitude control system using a magnet and oscillation dampers while it's power is derived from silicon solar cells and stored in a lithium ion battery. Instrumentation control, telemetry and data formatting are all accomplished with digital signal processors. The satellite should be ready for launch toward the end of 1998. [Ref 3]

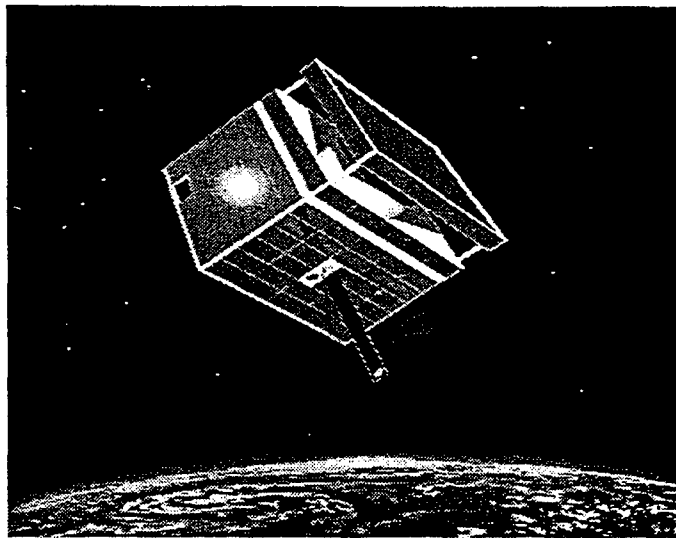


Figure B-1 - The Munin nanosatellite. From Ref. [27].

C. BITSY

Bitsy is a fully-functioned, autonomous, three-axis stabilized spacecraft in a 1 kg package. It features a single circuit board design which is easily tailored to specific mission requirements. Electrical power of 2-10 watts is supplied to the 8 volt bus by silicon solar cells and is stored in a rechargeable Lithium ion battery. Data handling is provided by a 32-bit microprocessor with off-the-shelf real-time operating system, common communication protocols and ANSI C language support. Bitsy is integrable with nearly every conceivable payload and can be operated by a single PC at a ground terminal. [Ref 29] Developed by the U.S. Air Force, Bitsy is now available for commercial applications in remote sensing, data message store and forward, space science and astrophysics and environmental monitoring. Bitsy is designed for flight only a few months after order and, like all nanosatellites, has significantly reduced launch and maintenance costs with only one million dollars required for a fully functioning turnkey system. [Ref 29] Bitsy is depicted in Figure B-2.

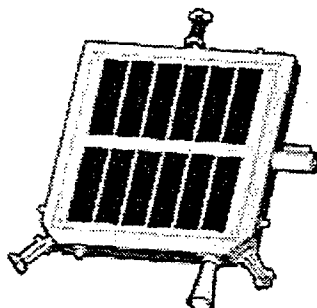


Figure B-2 - The Bitsy nanosatellite bus. From Ref [29].

D. ASUSat I

ASUSat I, shown in Figure B-3, has been developed by the Arizona State University (ASU) beginning in 1993 and is scheduled for launch in the second half of 1998 on either a Pegasus or Taurus launch vehicle. It is a 4.5 kg spacecraft which has been student-designed as a technology demonstrator for a low cost satellite. The satellite will be placed into a low earth polar orbit to provide earth imagery, an audio transponder for amateur radio operators and a proof of concept on a fluid damping method and attitude determination sensors. The lifetime of the satellite is approximately two years with all imagery and telemetry data being transmitted to the ground station at ASU.

E. TUBSAT SERIES

The TUBSAT nanosatellites, a project directed by the Technical University of Berlin, began in 1991 with TUBSAT-1 whose primary mission was academic research, particularly in the field of attitude determination. It was a cube weighing approximately 35 kg and was launched into a sun-synchronous orbit with an altitude of 780 km in 1991. It contained a three-axis star sensor, a fixed momentum wheel and magnetotorquer coil, a two-axis sun-sensor and three-axis magnetometer. [Ref 30]

TUBSAT-2, as shown in figure B-4, was launched in January of 1994 into an elliptical orbit of axis 1221x1198 km at an inclination of 83°. It included a second star sensor with a one meter focal length which also acted as a camera. The satellite was similar in design to TUBSAT-1 but included a 3 kg three axis reaction wheel and meteorological and radiation budget instruments.

The final satellite in the series is TUBSAT-C which will be launched next year and is reported to be used for testing laser ring gyros as a means of attitude determination and control. [Ref 30]

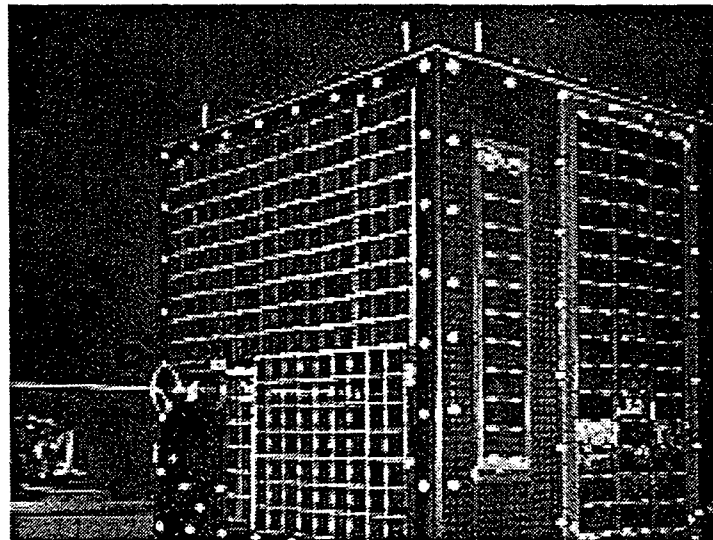


Figure B-3 - The TUBSAT-C nanosatellite. From Ref. [31].

F. SNAP-1

The SNAP nanosatellite is also a proof of concept satellite built by the engineers at University of Surrey Centre for Satellite Engineering research in England. It is a 2.5 kg and is shaped as a hexagonal prism. [Ref 3] It is powered by 48 GaAs solar cells which deliver an average power of one watt. It's payloads include two CMOS APD video cameras with

digital frame storage, an Orion GPS receiver and a diplexed quarter wave UHF monopole antenna to enable it to operate in the amateur radio band at an uplink/downlink of 9600 bps with frequency shift keying. [Ref 3]

LIST OF REFERENCES

1. Luscombe J.H., 1993, "Current Issues in Nanoelectronic Modeling" *Nanotechnology* 4, 1-20.
2. Larson W.J. and Wertz J.R., 1996, *Space Mission Analysis and Design* (Torrance: Microcosm Inc), pp. 340-357, 777-789.
3. Small Satellite HomePage, Internet
<http://www.ee.surrey.ac.uk/EE/CSER/UOSAT/SSHP>.
4. Payne, Robert A., *Applications of the Petite Amateur Naval Satellite*, M.S. Thesis, Naval Postgraduate School, Monterey, CA, 1992.
5. Lloyd's satellite constellations, "Iridium", Internet
<http://www.ee.surrey.ac.uk/Personal/L.Wood/constellations/iridium.html>
6. Kenny, T.W. et al., 1992, "Electron Tunneling Sensors" *J.Vac. Sci. Technol. A* (Jul./Aug. 1992).
7. Smit, G.N., 1993, "Nanotechnology for Guidance, Navigation and Control" Aerospace Report No. ATR-93(8349)-1 pp. 13-19.
8. Radhakrishnan, G., 1993, "Microsensors and Microinstruments for Guidance, Navigation and Control" Aerospace Report No. ATR-93(8349)-1 pp 23-27.
9. Cassady, R.J., Meckel, N.J., and Hoskins, W.A., 1996, "Pulsed Plasma Thruster Systems for Spacecraft Attitude Control" A paper delivered at the AIAA Conference on Small Satellites.
10. Tilley, D.L., Pobst, J.A., and Bromaghim, D.R, 1996, "Advanced Pulsed Plasma Thruster Demonstration on MightySat Flight II.1" A paper delivered at the AIAA Conference on Small Satellites.
11. Gilmore, D.G., 1993, "Nanotechnology for Spacecraft Thermal Control" Aerospace Report No. ATR-93(8349)-1 pp. 49-58.
12. Berry, E.R., 1993, "Miniaturizing Spacecraft Power and Electrical Systems" Aerospace Report No. ATR-93(8349)-1 pp. 57-59.
13. Caldwell, D.B., Fox, C.L., and Miller, L.E. "Powering Small Satellites with Advanced NiH₂ Dependent Pressure Vessel (DPV) Batteries" A paper delivered at AIAA.

14. Eisele, Anne, "JPL Explores New World of Tiny, Smarter Electronics," *Space News*, 30 March-5 April, 1998.
15. Turton, Richard, 1995, *The Quantum Dot*, (New York: Oxford University Press).
16. Seabaugh, A.C., Luscombe, J.H., Randall, J.N., 1993, "Quantum Functional Devices: Present Status and Future Prospects" *FED Journal* 3, pp. 9-17.
17. Reed, Mark A., *Quantum Dots*, Scientific American, January 1993, pp. 98-104.
18. Kruppa, Suzanne, *Modeling the Quantum Dot*, M.S. Thesis, Naval Postgraduate School, Monterey, CA, 1997.
19. Resnick R. and Halliday D., 1993, *Fundamentals of Physics*, (New York: John Wiley and Sons), pp. 1219-1221.
20. Sze S.M., 1985, *Semiconductor Devices, Physics and Technology*, (New York: John Wiley and Sons), pp. 71-80.
21. Isakowitz, Steven J., 1995, *Space Launch Systems*, (Washington D.C.: AIAA), pp. 201-175.
22. Orbital Sciences Corporation, "Photo Gallery", Internet http://www.orbital.com/Prods_n_Servs/Products/LaunchSystems/Pegasus/expanded.html
23. Orbital Sciences Corporation, Internet http://www.orbital.com/Prods_n_Servs/Products/LaunchSystems/Taurus/index.html
24. Vandenberg Air Force Base marketing, Internet:
<http://www.vafb.af.mil/orgs/xp/xpr/MARKET/Scout.htm>
25. Patterson Air Force Base marketing, Internet:
<http://www.pafb.af.mil/450G/45wa/titan1gf.htm>
26. Delta II Launch Photos "A Delta II 7920-10 Iridium launch" Internet:
<http://violet.pha.jhu.edu/photos/delta.html>
27. My Shuttle Launch Pictures, Internet <http://www.hal-pc.org/~kg5u/0413g.html>
28. The Munin satellite homepage, Internet: <http://munin.irf.se/>
29. The AeroAstro Corporation Homepage, Internet: <http://www.aerospace.com>

30. Small Satellite Homepage, Internet:
http://www.ee.surrey.ac.uk/EE/CSER/UOSAT/SSHP/future_nanos.html
31. Small Satellite HomePage Internet
<http://www.ee.surrey.ac.uk/EE/CSER/UOSAT/SSHP/pix/tubsat1a.gif>

INITIAL DISTRIBUTION LIST

1. Defense Technical Information Center.....2
8725 John J. Kingman Rd., STE 0944
Fort Belvoir, VA 22060-6218
2. Dudley Knox Library.....2
Naval Postgraduate School
411 Dyer Rd.
Monterey, CA 93943-5101
3. Professor J.H. Luscombe, Code Ph/Lj.....2
Department of Physics
Naval Postgraduate School
Monterey, CA 93943-5002
4. Lt. Jack Rice.....2
2052 Quaker Way #5
Annapolis, MD 21401